Pergamon

Int. J. Heat Mass Transfer. Vol. 40, No. 11, pp. 2637–2645, 1997

Printed in Great Britain
0017–9310/97 $17.00+0.00

PII: S0017-9310(96)00279-7

Thermal boundary resistance for thin-film high-T_c superconductors at varying interfacial temperature drops

MUKUL KELKAR, PATRICK E. PHELAN†‡ and BEI GU†

Department of Mechanical Engineering, University of Hawaii at Manoa, 2540 Dole Street H302, Honolulu, HI 96822, U.S.A.

(*Received* 27 *July* 1995 *and in final form* 5 *August* 1996)

Abstract—High-temperature thin-film superconducting devices are becoming commonplace for applications such as Josephson junctions, superconducting quantum interference devices, interconnects and radiation bolometers. The thermal stability of these devices is critical and for effective heat transfer it is required to know the thermal boundary resistance at the interface of the high-T_c thin films and their substrates. Many measurements of thermal contact resistance for bulk samples and metallic thin films have been reported, but only a few measurements have been made for high-T_c films. In the present study, the thermal boundary resistance between Er–Ba–Cu–O films on MgO and $SrTiO_3$ substrates is measured as a function of both temperature and the applied heat flux, and for the first time at temperatures as low as 19 K. The boundary resistance shows a decrease with increasing heat flux. Possible explanations for this trend are given by three proposed hypotheses.

INTRODUCTION

The thermal boundary resistance (R_b) between a superconducting thin film and the substrate can strongly affect the thermal design of high-T_c devices. A restriction for heat flow from the film can cause a transition from the superconducting state to the normal state during operation of the device, resulting in device failure. High-T_c applications such as Josephson junctions, interconnects and flux flow transistors [1] are dependent on the thermal stability of the films and require knowledge of R_b and its variation with heat flux, such as from heat generation within electronic chips. The time constant in the bolometric response of a high-T_c superconductor depends on R_b which makes it important for the design of radiation detectors [2, 3]. A few direct measurements of R_b have been reported [4–7]. These measured values of R_b range between 0.5×10^{-3} and 5×10^{-3} K cm^2 W^{-1} and generally show a slight increase with temperature. No variation with heat flux has been reported in the past for thin films. In this paper we discuss primarily the effect of the heat flux, or equivalently, the interfacial temperature drop, on R_b.

EXPERIMENT

Samples

The R_b of three Er–Ba–Cu–O samples has been measured. Sample 1 is 70 nm thick on MgO substrate with a T_c of approximately 69 K; sample 2 is 300 nm thick on $SrTiO_3$ substrate with a T_c of 89 K and sample 3 is an oxygen-deficient 70 nm thick film on MgO substrate. We are not able to determine the T_c of the third sample even down to 19 K, the cooling limit of our cryogenic cooling apparatus. The characteristics of the three samples are summarized in Table 1. The substrate thickness for all samples is 1 mm. The films were made by ionized cluster beam codeposition [8] and etched in a meander pattern as shown in Fig. 1 [5, 6].

Procedure

The experimental procedure is based on that described by Swartz and Pohl [9–11], and is fully described in Refs. [5, 6]. A large current is passed through the wider (heater) strip shown in Fig. 1, and a much smaller sensing current is passed through the narrower (sensor) strip. Joule heating provides a temperature difference between the heater and the substrate. While the heat flux is measured directly from the heater electrical current and voltage drop, the temperature of the film and the substrate need to be indirectly determined. If a very small sensing current is passed through the narrower (sensor) strip, then its temperature is approximately equal to that of the substrate due to its insignificant Joule heating. Separately, the electrical resistances of the two strips are measured with small sensing currents by the four-point method and plotted against temperature under isothermal conditions, as shown in Fig. 2. Calibration curves in the reverse plot of temperature vs electrical resistance allow us to determine the film temperatures

† Present address: Department of Mechanical and Aerospace Engineering, Arizona State University, Tempe, AZ 85287-6106, U.S.A.

‡ Author to whom correspondence should be addressed.

NOMENCLATURE

A	nominal interfacial area
A^+	enhanced interfacial area
c	sound velocity
h_c	thermal contact conductance [W cm^{-2} K^{-1}]
H	Vickers microhardness
j	mode of vibration
k_B	Boltzmann constant [1.38062×10^{-23} J K^{-1}]
k_m	harmonic mean thermal conductivity [W cm^{-1} K^{-1}]
K	empirical constant
m	empirical constant
n	power index
N	phonon number density
q	heat flux [W cm^{-2}]
Q	heat transfer [W]
R	thermal resistance [K cm^2 W^{-1}]
R_b	thermal boundary resistance [K cm^2 W^{-1}]
T	temperature [K]
ΔT	temperature drop [K]
$\delta(\Delta T)$	error in temperature calibration [K]
P	apparent interfacial pressure [GPa].

Greek symbols

α	transmission coefficient
Δ	change
γ	area enhancement factor
Γ	transmission probability function
θ	phonon incidence angle
σ	surface roughness
ω	frequency
$\hbar$	Planck's constant/2π.

Subscripts

1	side 1
2	side 2
c	critical
D	Debye
h	heater
s	sensor
m	mean.

Table 1. Sample characteristics

Sample	Substrate	Film thickness [nm]	T_c [K]	Range of heat flux (W cm^{-2}]	Substrate temperature range [K]
1	MgO	70	69	200–800	110–240
2	$SrTiO_3$	300	89	20–200	100–230
3	MgO	70	—	1–150	20–210

from their measured electrical resistances. The temperature drop in the substrate between the two strips is calculated using the thermal conductivity of the substrate and is accounted for while determining R_b. When steady-state is reached, R_b is defined as

$$R_b = \frac{T_h - T_s}{q} \quad (1)$$

where T_h is the average heater temperature, T_s the average sensor temperature and q is the heat flux.

These experiments were carried out in a closed cycle refrigeration system attached to a computer controlled data acquisition system. The sample was mounted to the surface of a copper cold finger, and was surrounded by vacuum. The imposed heat flux ranged from 200–800 W cm^{-2} for sample 1, 20–200 W cm^{-2} for sample 2 and 1–150 W cm^{-2} for sample 3. The sensing current was 10 μA-ac. The temperature during the calibration procedure was measured by a Si diode which was thermally connected by Apiezon

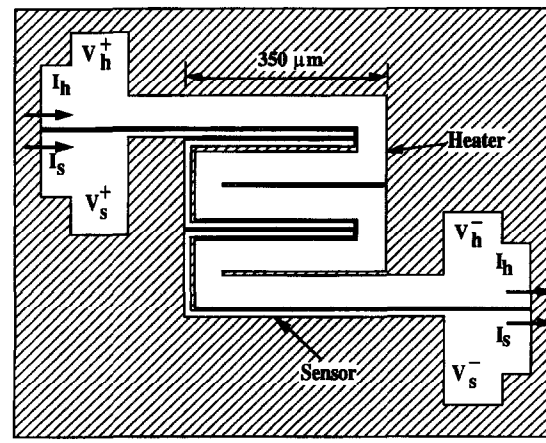

Fig. 1. Two-strip meander etch pattern of the high-T_c thin film. The width of the heater strip is 50 μm, that of the sensor strip is 10 μm and the separation is 5 μm.

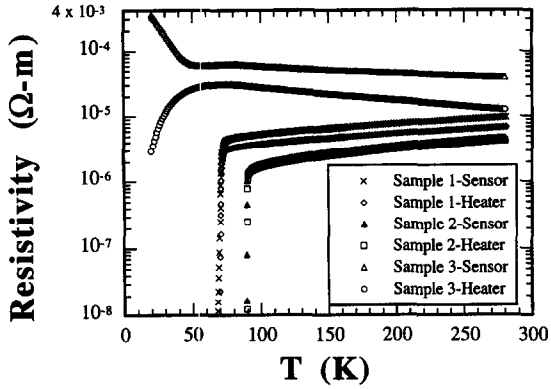

Fig. 2. Calibration plot of resistivity vs temperature.

grease to the cold finger in the cryogenic refrigeration system.

Error analysis

We attribute errors in our measurements to three major causes: firstly, the heat leak through the electrical connection leads, secondly the temperature drop in the substrate and lastly, the uncertainty in the calibration curves. Heat loss due to radiation and errors due to Joule heating at the contact pads, which are minor, have also been determined.

The heat leak through the leads is determined by considering the different paths of heat flux and estimating the flow in each path. An equivalent thermal circuit diagram is made and a two-dimensional heat conduction solution gives the ratio of the heat leak to effective heat transfer as 0.16. The resulting percent heat leak is 13.7%.

The uncertainty in the calibration curves for T_h and T_s is determined from the standard deviation of the curve fits to the plots of electrical resistivity vs temperature of Fig. 2. The uncertainty δ in ΔT is $\delta(\Delta t) < 0.41$ K for sample 1 and $\delta(\Delta T) < 0.17$ K for sample 2. Since the ΔT for sample 3 is very large, the fitted curves give a very low % error. The heat flux uncertainty is 5% as a standard error of the current from the Keithley current source.

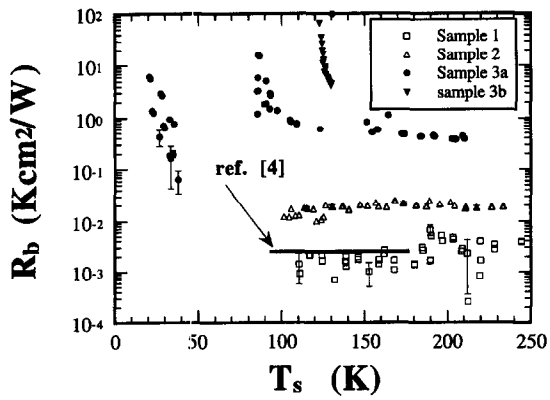

Fig. 3. Thermal boundary resistance vs sensor temperature for all data points for the three samples.

The temperature drop across the substrate, between the heater and sensor strip, affects the calculation of R_b and leads to a value of R_b higher than the actual one. This temperature drop needs to be determined and subtracted from all calculations to obtain a corrected value for R_b. The substrate thermal conductivity at different temperatures and two-dimensional heat conduction is used for the calculations. The effect is small at low temperatures and low heat fluxes, and for sample 3 is negligible due to its large temperature drops. The temperature drop across the thin film is also calculated and determined to be negligible.

The radiation heat loss from the film to the surrounding brass shroud is very low. The electrical contact resistance at the connection pads, which can cause Joule heating, is measured to be about 140 Ω by a two-resistance technique. This extra generated heat is included in the uncertainty of R_b, which is shown as error bars for representative data points in the figures.

RESULTS AND DISCUSSION

The thermal boundary resistance between two surfaces causes a temperature discontinuity and occurs due to phonon scattering at the interface if one of the solids is nonmetallic. Such a contact resistance was studied extensively for the Kapitza helium boundary and the Acoustic Mismatch Model was used to explain this temperature discontinuity [10]. Little modified the theory for the solid–solid interface and predicted values in close agreement with the observations at low temperatures [10, 12]. There was, however, a substantial deviation at higher temperatures.

We have measured the boundary resistance for thin-film superconductors in their normal state deposited on single crystal substrates. Measurements of R_b for high-T_c films at temperatures as low as 19 K are reported for the first time. The oxygen deficient sample on MgO enables these measurements since it remains normal throughout the measured temperature range. During measurement at these low temperatures, we observe a characteristic effect of the heat flux on R_b. Experiments are also performed at higher temperatures and a similar effect is observed.

A plot of electrical resistivity vs temperature is given in Fig. 2 for the three samples. The resistivity plots indicate a T_c of 69 K for sample 1 and 89 K for sample 2. For sample 3, the resistivity shows an increase with a decrease in temperature, which is probably due to low oxygen content. For the heater strip, this decreases again while it becomes very large for the sensor strip. A similar increase has also been observed for bulk samples [13]. From the calibration curve, it is difficult to determine exactly the temperatures around the peak for the heater plot and, hence, no measurements are reported from 50 K to 80 K for that sample. Since sample 3 is very resistive, high currents cannot be imposed because of the limitation of our current source.

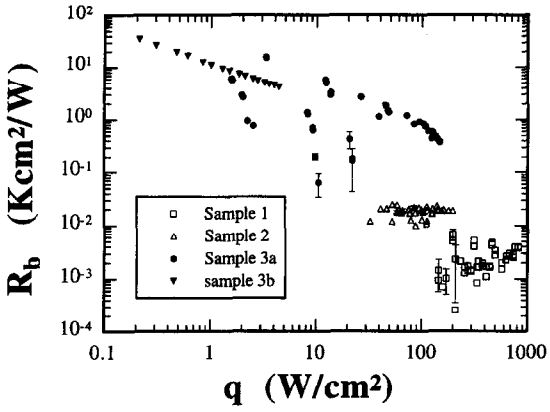

Fig. 4. Effect of heat flux on R_b for all data points.

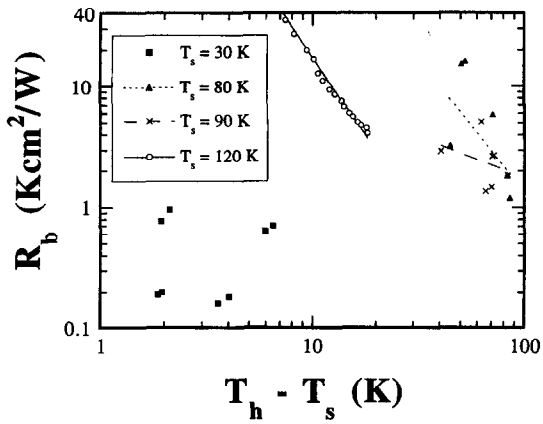

Fig. 5. Effect of ΔT on R_b at constant T_s for sample 3.

The plot of R_b against temperature for the three samples is shown in Fig. 3. A comparison of R_b between the oxygen deficient sample 3 and the other samples shows a vast difference with the values in the deficient sample being three orders of magnitude greater. Such large values of R_b have not been observed before for thin films and we believe it to be a manifestation of the high oxygen deficiency and perhaps a lower film quality. Some measurements for sample 3 were made after a 2 month hiatus and a significant increase in the magnitude of R_b was consequently observed. We believe that the film degraded further and the oxygen deficiency was further increased. To distinguish between the two measurements, we label all measurements at the earlier date, with the lower oxygen deficiency, as sample 3(a) and the later measurements as sample 3(b). A comparison of our measurements is made with Ref. [4] and the data of sample 1 are in close agreement, while those of sample 2 and 3 are much higher. We expect the magnitude of R_b to be lower for sample 2, since the film is deposited on $SrTiO_3$ substrate which has a better lattice match with the high-T_c film compared to MgO. The greater thickness of the film and the lower thermal conductivity of $SrTiO_3$ compared to MgO may possibly contribute to the higher magnitudes measured. The case of the film actually being separated from the substrate is considered by assuming black body radiation between the film and the substrate, which yields a value of R_b as high as 10^4 K cm^2 W^{-1}. This suggests not a separated, but rather a poorly deposited film. The scatter for sample 3 is very large, which could be a manifestation of different heat fluxes.

Figure 4 shows the variance of R_b with heat flux for all three samples at different temperatures. A decreasing trend is observed and is especially noticeable for sample 3. As the applied heat flux increases, the temperature drop (ΔT) across the interface increases and hence we also observe a decrease in R_b with increasing ΔT. Some representative values of R_b at a constant temperature ($T_s \pm 5$ K) are plotted on a logarithmic scale vs ΔT in Fig. 5 for sample 3 and on a linear scale

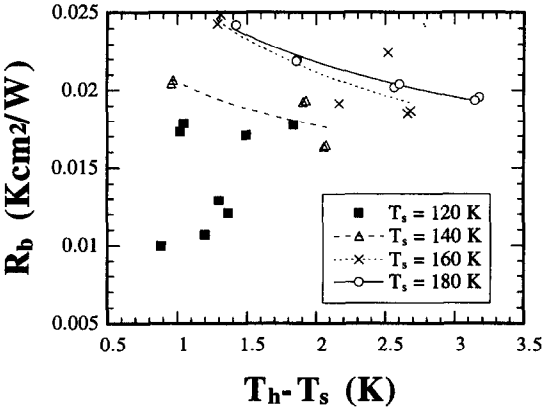

Fig. 6. Effect of ΔT on R_b at constant T_s for sample 2.

Table 2. Curve fit coefficients and equations for R_b as a function of ΔT, at constant substrate temperatures

T_s [K]	Equation
	Sample 3
80	$R_b = 32295 * \Delta T^{-2.1921}$
90	$R_b = 38.47 * \Delta T^{-0.66868}$
120	$R_b = 6718.8 * \Delta T^{-2.5899}$
	Sample 2
140	$R_b = 0.020555 * \Delta T^{-0.21522}$
160	$R_b = 0.026644 * \Delta T^{-0.33108}$
180	$R_b = 0.02626 * \Delta T^{-0.2674}$

in Fig. 6 for sample 2. We observe an almost power law decrease of R_b with ΔT. Table 2 shows the curve fit equations of the form $R_b = y \cdot (\Delta T)^n$ at different sensor temperatures for samples 2 and 3. The power law decrease is not observed for sample 3 at $T_s = 30$ K and for sample 2 at $T_s = 120$ K. The scatter in the sample 1 data does not allow us to segregate data points to observe the effect of ΔT and, hence, those values are not presented here.

Kashani and Sciver [14] measured the Kapitza conductance of technical copper samples with different surface preparations. A variation of the surface temperature with heat flux as well as the limiting values

of Kapitza conductance for a small temperature difference were determined in the study. The plots of the surface temperature of the samples against heat flux showed a decrease in their slope. If the surrounding temperature is assumed constant, this would indicate a decreasing contact resistance with increasing heat flux, in accord with the results in Figs. 5 and 6. Satter and Ashworth [15] suggested a decrease of thermal boundary resistance with increasing heat flux for a thin nylon sample on copper. They also presented their data graphically showing the decreasing trend, but the error bars were large. Balcevic and Bolsaitis [16] gave values of the thermal contact resistance at high heat fluxes for bulk samples. They observed a decrease in R_b with increasing contact pressure but show no dependence of heat flux. In our measurements, the plot of R_b vs heat flux, or temperature drop, levels off and we also observe an almost constant R_b at high magnitudes of heat flux, as seen in Figs. 4–6. Fletcher [17] discussed some related effects of the heat flux and contact pressures on the contact conductance.

Three hypotheses are proposed to explain the effect of the temperature drop (or equivalently, heat flux) on the measured R_b. The first is based on the change in peeling stress generated due to thermal stresses in the film, the second on microscale heat transfer effects and the third from the T^4 dependence of heat transfer as derived from the acoustic and diffuse mismatch theories.

Explanation based on peeling stress

When thermal transport across interfaces is modeled, most often, a perfect contact of the two solids is assumed. The interface formed due to the joining of two solids is represented in different ways in Fig. 7. Practical situations appear as in Fig. 7(b, c).

To measure R_b, the contact area at the interface needs to be determined. A larger area provides a greater path for heat transfer and thus reduces the contact resistance. The application of a heat flux across the interface raises the temperature of both the lattices and also causes a temperature drop. The differential thermal expansions results in a change in the contact pressure between the two solids. This change in contact pressure, if positive, causes the film to press onto the substrate by elastic (or plastic) deformation, thereby increasing the contact area. A film–substrate interface upon thermal expansion may change as in Fig. 7(b) to that in Fig. 7(c).

The effect of contact pressure on heat transfer across interfaces and thermal boundary resistance (or contact conductance) has been observed in many studies on bulk samples [17–20]. There is a direct dependence of the contact conductance on the interfacial pressure. The relation between conductance and contact pressure is typically given as [20–21].

$$\frac{h_c\sigma}{k_m} = c\left(\frac{P}{M}\right)^n \tag{2}$$

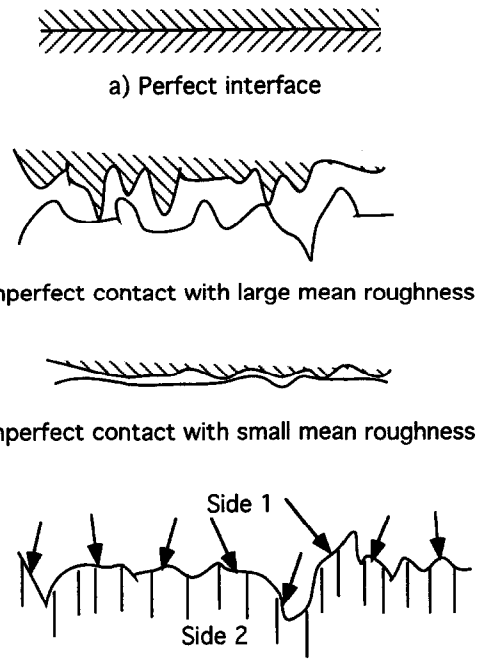

Fig. 7. Different types of interfaces.

where h_c is the thermal contact conductance, σ the surface roughness, k_m the harmonic mean thermal conductivity, P the apparent interfacial pressure, H the Vickers microhardness and c and n are empirical constants. Though this equation is primarily derived for plastic deformation, Mikic [20] explains that the constants are very similar for the elastic case as well.

Typical curves fitted to experimental data for two metal surfaces [21] changes equation (2) to

$$\frac{h_c\sigma}{mk_m} = 1.25\left(\frac{P}{H}\right)^{0.95} \tag{3}$$

where m is the mean profile slope.

Such a relation, specifically for the interface of uncoated bulk BiCaSrCuO superconductor and copper at cryogenic temperatures, was given by Ochterbeck *et al.* [2] as

$$\frac{h_c\sigma}{k_m} = 5.25\times10^{-4}\left(\frac{P}{H}\right)^{0.51}. \tag{4}$$

The relationship between R_b and the contact pressure for these bulk samples is a reciprocal of the relationships given in equations (2)–(4), since $R_b = 1/h_c$. No study so far has been done on the effect of applied pressure on thermal contact resistance of the interface of thin films on single-crystal substrates. An empirical relationship between the resultant peeling stress in thin films and R_b is suggested.

The formation of residual stresses in thin-film high-temperature superconductors during *in situ* processing was modeled and calculated by Phelan and Ghasemi

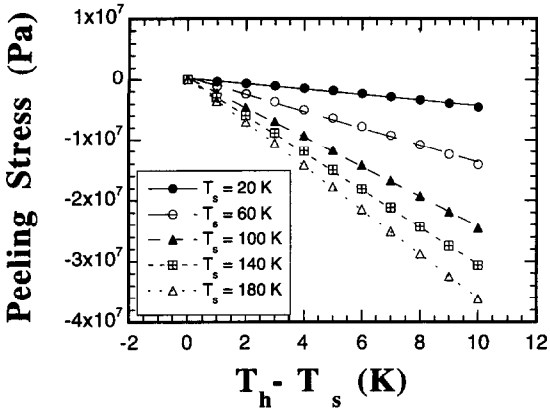

Fig. 8. Change in peeling stress at the film–substrate interface with increasing temperature difference.

Nejhad [22]. They represented the film-substrate system as a multi-layered, multi-ply asymmetric laminate. The *in situ* unrestrained processing strains were a sum of the thermal expansion strains and the chemical shrinkage strains. The residual stresses due to this chemical shrinkage and the cooling from the processing temperatures (~ 630 K) to the operating temperatures (~ 50 K) were calculated. A so-called *peeling* stress, normal to the interface, was defined as a resultant of the residual stresses in the bordering layers in the film and substrate. The films used in the presently studied samples were annealed after deposition and hence the effect of chemical shrinkage is not considered. The change in peeling stress generated by the temperature difference between the film and substrate is calculated using the model of Phelan and Ghasemi Nejhad [22].

Figure 8 shows a plot of the calculated change in peeling stress, Δp, with an increase in the temperature drop between the film and the substrate for the Er–Ba–Cu–O/MgO system. Suhir [23] presented an approximate expression for the peeling stress at the interface of multilayered elastic films, and calculations using this expression show the same trend as the results from the Phelan and Ghasemi Nejhad model. Figure 8 indicates that the relative change in peeling stress increases with increasing temperature due to the temperature dependence of the material properties. The ΔP for the film/substrate interface, when the film is heated to a temperature ΔT greater than that of the substrate, can be represented by the relation

$$\Delta P \propto (\Delta T) \quad \text{or} \quad \Delta P = m(\Delta T) \tag{5}$$

since Fig. 8 shows that for all values of T_s, the peeling stress decreases linearly, i.e. becomes more compressive, with increasing $\Delta T = T_h - T_s$.

If equation (2) is coupled with equation (5), and noting that $R_b = 1/h_c$, we get

$$R_b = A \cdot (\Delta P)^{-n} \tag{6}$$

where A and n are constants. In particular, because of this linear dependence of ΔP on ΔT, the exponent "n" has the same meaning as those in equations (2)–(4), and thus our data can be compared directly with those previous results.

From Table 2, we can see that the typical measured values of "n" for sample 2 range from -0.2 to -0.35 and for sample 3 from -0.6 to -2.5. The power indexes for sample 3 are much higher and for sample 2 are much lower than those in the general expression for the contact conductance (equations (3) and (4)). This is the first time that a contact pressure approach has been applied to explain the R_b at the interface of thin films and their substrates. Since the films are physically deposited by sputtering or laser ablation, they result in a very uniform interface in contrast to the interface of bulk samples. There may actually be a local displacement in the lattice and filling of defects which causes the change in the effective interfacial area. The dependence of R_b on the interfacial pressure here is different than for the bulk metallic or superconducting samples [21].

Explanation on the basis of microscale heat transfer

The basis of this theory is the discussion by Little [12] on heat transfer in dielectric solids which is dominantly by phonons [24]. At the interface there is a scattering of phonons which gives a resistance to heat flow. The long wavelength and long mean free path phonons can carry heat more effectively across an interface [25]. Consider an actual interface with gaps in the contact zone as shown in Fig. 7(b). The long wavelength longitudinal lattice waves would move in phase between these contact points at large distances, but the high energy phonons, with wavelengths much smaller than these separations, would be scattered. The scattering would depend on the actual separation between the two lattices at that point. Point defects and boundaries also constitute a major source of phonon scattering, which affect their mean free path. The number density of excited phonons is proportional to temperature and at high temperatures all phonon modes are excited [26].

The films are deposited by rf-sputtering to a thickness of the order 10^3 Å. At this small dimension it is possible for the films to cover the undulations in the substrate due to its inherent roughness. For such an idealized case of the film–substrate interface as shown in Fig. 7(d), the contact area is actually greater than the area of contact in the perfect interface of Fig. 7(a).

For high energy (low wavelength) phonons with a mean free path of the order of the surface roughness, the effective area becomes an integrated microscopic area of the interface. If the wavelength of the phonons is large, then they see the geometric area, thereby reducing the heat transfer [12].

The quantized energy of a phonon is given as $h\omega$ [26]. A supply of heat to the lattice increases the energy of the phonons which leads to an increase in high frequency and low wavelength phonon concentrations. For the interfaces considered, long wave-

length phonons would see only the geometric area, but the short wavelength phonons would see an integral of the microscopic area. Thus there is a greater effective area for the transport of high frequency phonons than for the long wavelength phonons.

Little [12] explains in detail the heat transfer across an interface between dissimilar solids and gives an expression for the net heat transfer Q as

$$Q = \frac{1}{2}\sum_j \int_A \int_{\theta=0}^{\pi/2} \int_{\omega=0}^{\omega_{D1}} N_1(\omega, T_1, j)\hbar\omega c_{1j}\alpha_{1-2}(\theta, j) \times \cos\theta \sin\theta \, d\omega \, d\theta \, dA - \frac{1}{2}\sum_j \int_A \int_{\theta=0}^{\pi/2} \int_{\omega=0}^{\omega_{D2}} N_2(\omega, T_2, j)\hbar\omega c_{2j}\alpha_{2-1}(\theta, j) \times \cos\theta \sin\theta \, d\omega \, d\theta \, dA \quad (7)$$

where N is the phonon number density, θ the phonon incidence angle, ω the phonon frequency, α the transmission coefficient, c the velocity of sound in the medium, A the geometric or nominal interfacial cross sectional area and $\hbar$ is Planck's constant/2π.

The substrate temperature (T_2) is kept constant and any increase in heat flux is assumed to increase the film temperature (T_1). For the considered interface, due to an increase in energy and thus a decrease in wavelength an increase in area is observed on the film side. If the geometric nominal area is denoted as A and it is assumed that all phonons on side 2 see this nominal area, then due to an increase in temperature T_1, all film phonons would see a net microscopic area grater than A, say A^+. Thus the first term in equation (7) would be increased by a factor of γ, where $\gamma = A^+/A$, thereby increasing the Q. This means that an increase in the *heat flux* causes an increase in the *net heat transfer*. An approximate relationship can thus be derived for this effect of enhanced area on R_b.

The expression for experimentally measured R_b in equation (1) can be written as

$$R_b = \frac{\Delta T}{q} = \frac{\Delta T}{Q/A} \quad (8)$$

where Q and A are defined above.

A heat flux q when applied to the film causes an increase in A^+, the interfacial microscopic area. The ratio of A^+ to A, introduced earlier, is defined as the area enhancement factor γ. The heat flux across this increased interfacial area is called q_{enhanced}. The boundary resistance due to the net effect of the microscopic area at the interface is termed $R_{b,\text{enhanced}}$ and is given as

$$R_{b,\text{enhanced}} = \frac{\Delta T}{q_{\text{enhanced}}} = \frac{\Delta T}{Q/A^+}. \quad (9)$$

From the definition of γ we can modify equation (9) to get

$$R_{b,\text{enhanced}} = \frac{\Delta T}{Q/\gamma A} = \frac{\gamma \Delta T}{Q/A} = \frac{\gamma \Delta T}{q} = \gamma R_b \quad (10)$$

which gives us an expression for the experimentally measured R_b as:

$$R_b = \frac{R_{b,\text{enhanced}}}{\gamma}. \quad (11)$$

If it is assumed that the microscopic boundary resistance remains the same throughout, then any increase in q increases γ, which would result in a decrease in the measured R_b as per equation (11). It is useful to note that R_b decreases inversely with γ, i.e. inversely with q, which is similar to our experimental observations.

Explanation on the basis of T^4 *dependence of* R_b

The expression for net heat transfer based on the acoustic mismatch theory, equation (7), can be integrated to obtain the following expressions. At small T_1 and T_2 we derive [12]

$$q = \frac{Q}{A} = \frac{\pi^2 k_B^4}{60\hbar^3}\sum_j [c_{1j}^{-2}\Gamma](T_1^4 - T_2^4) \quad (12)$$

and at large T_1 and T_2 we have [12]

$$\frac{Q}{A} = \frac{k_B \omega_D^3}{12\pi^2}\sum_j [c_{1j}^{-2}\Gamma](T_1 - T_2) \quad (13)$$

where Γ is an integrated transmission function depending on the sound velocities and the transmission coefficients of the two media.

For the assumption of constant material properties over the temperature ranges considered, equations (12) and (13) can be rewritten as

$$q = \frac{Q}{A} = K_1(T_1^4 - T_2^4) \quad (14)$$

$$q = \frac{Q}{A} = K_2(T_1 - T_2) \quad (15)$$

where K_1 and K_2 are constants evaluated on the basis of the material properties and Γ is obtained from the appendices of Ref. [27].

If T_1–T_2 is denoted as ΔT, then

$$T_1^4 - T_2^4 = \Delta T(2T_2 + \Delta T)(2T_2^2 + \Delta T^2 + 2T_2\Delta T). \quad (16)$$

Combining equations (14) and (15) in equation (1), we can write for high and low temperatures

$$R_b(\text{low}) = \frac{\Delta T}{q} = \frac{1}{K_1(2T_2 + \Delta T)(2T_2^2 + \Delta T^2 + 2T_2\Delta T)} \quad (17)$$

$$R_b(\text{high}) = \frac{\Delta T}{q} = \frac{1}{K_2}. \quad (18)$$

It is observed by experiments that R_b becomes con-

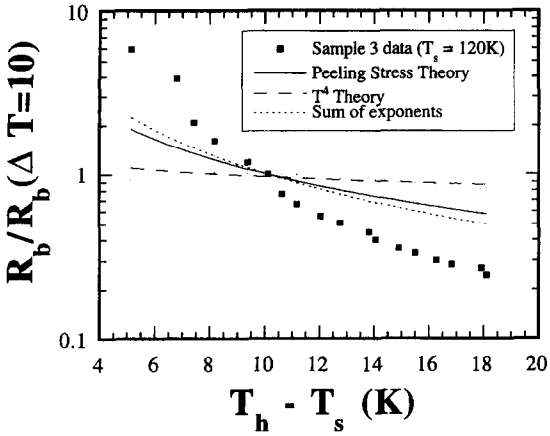

Fig. 9. Comparison of theory with data for sample 3.

stant at high temperatures, while it is a function of q or ΔT at low temperatures. A plot of $R_b * K_1$ vs ΔT for different substrate temperatures yields a dependence of R_b on ΔT of $R_b \sim (\Delta T)^{-0.2}$. Note that the term $R_b * K_1$ is not a function of the substrate material. A similar T_4 dependence is also observed from equations based on the diffuse mismatch model [11].

Comparison with experimental data

The theories proposed above are compared to the data of sample 3 at a sensor temperature of 120 K. Figure 9 shows a plot of a nondimensionalized R_b vs the temperature drop. The nondimensionalization is done by dividing all values with a reference value at $\Delta T = 10$ K and is necessary in order to easily compare the trends of the data and the proposed theories. A curve for the microscale heat transfer theory is not shown since an explicit dependence of R_b on ΔT could not be derived for that theory. Instead, a plot like Fig. 9 will yield empirical information about the dependence on γ, as discussed below.

A power law fit to the data of sample 3 indicates an exponent of -2.2. The exponent in the T^4 dependence curve is -0.2 and that from the peeling stress curve, assuming a relationship like equation (3), is -0.95. The theories individually indicate an index smaller than the observed trend of the data. A curve with the sum of the indexes of the two theories is also plotted and shows an improved match with the experimental data. In some sense, sample 3 is a worst case scenario in that it has the highest index amongst the three samples and thus the fits for the other samples are better. The microscale effect would presumably add to the exponent. Based on this assumption, a comparison between the experimental data in Fig. 9 and the sum of the three theories yields an additional value for the R_b dependence on ΔT as ~ -1. From this and equation (11) we can deduce that γ is almost a linear function of ΔT. Fits to other data at different temperatures would yield different values of dependence on γ. Thus a sum of the exponents obtained from the three theories would explain the measured data more accurately, and it is suggested that an approximate equation derived from all three theories is possible. Future work will concentrate on providing better characterized experimental data that will allow such a quantitative theory to be developed.

CONCLUSIONS

The film–substrate thermal boundary resistance is measured for three Er–Ba–Cu–O films as a function of temperature and the interfacial temperature drop. All measurements are carried out in the normal state and for different substrates and varying film thicknesses. Measurements are made for the first time at temperatures as low as 19 K. The results indicate an R_b greater than 10^{-3} K cm^2 W^{-1} for the first sample, 10^{-2} K cm^2 W^{-1} for the second sample and 10^{-1} K cm^2 W^{-1} for the third sample. The large values for sample 3 are thought to be due to the poor quality of the film. R_b also shows a decreasing trend with increasing heat flux and interfacial temperature drop. Possible explanations for this effect are discussed in the form of three hypotheses: a thermal stress effect, a microscale heat transfer effect and the effect of the T^4 dependence of heat transfer. A combination of the three hypotheses attempts to explain the trends in the data.

Acknowledgements—This material is based upon work supported by the National Science Foundation under Grant no. CTS-9696002. The authors owe their gratitude to Professor K. Hijikata of the Tokyo Institute of Technology and H. Ito of the Mitsubishi Electric Company, who furnished the high-T_c samples and to Professor J. R. Gaines of the University of Hawaii, who allowed us to use his cryogenic laboratory facilities.

REFERENCES

1. Bourdillon, A. and Tan Bourdillon, N. X., *High Temperature Superconductors: Processing and Science*. Academic Press, Inc., San Diego, CA, 1993.
2. Carr, G. L., Quijada, M., Tanner, D. B., Hirchmugl, C. J., Williams, G. P., Etemad, S., Dutta, B., DeRosa, F., Inam, A., Venkatesan, T. and Xi, X., Fast bolometric response of high-T_c detectors measured with subnanosecond synchrotron radiation. *Applied Physics Letters*, 1990, **57**(25), 2725–2727.
3. Levey, C. G., Etemad, S. and Inam, A., Optically detected transient thermal response of high-T_c epitaxial films. *Applied Physics Letters*, 1992, **60**(1), 126–128.
4. Nahum, M., Verghese, S., Richards, P. L. and Char, K., Thermal boundary resistance for $YBa_2Cu_3O_{7-d}$. *Applied Physics Letters*, 1991, **59**(16), 2034–2036.
5. Phelan, P. E., Song, Y. and Kelkar, M., Film/substrate thermal boundary resistance of Er–Ba–Cu–O high-T_c thin films. *Ceramic Transactions*, Vol. 41, *Symposium on Grain Boundaries and Interfaces in Electronic Ceramics*, 1993 PAC RIM Meeting of the American Ceramic Society, 1994, pp. 307–314.
6. Phelan, P. E., Song, Y., Nakabeppu, O., Ito, K., Hijikata, K., Ohmori, T. and Torikoshi, K., Film/substrate thermal boundary resistance for an Er–Ba–Cu–O high-T_c superconducting film. *Journal of Heat Transfer*, 1994, **116**(4), 1038–1041.

7. Zeuner, S., Lengfellner, H. and Prettl, W., Thermal boundary resistance and diffusivity for $YBa_2Cu_3O_{7-d}$ films. *Physical Review B*, 1995, **51**(17), 11903–11908.
8. Yamanishi, K., Yasunaga, S., Kawagoe, Y., Sato, K. and Imada, K., Synthesis of superconducting Y–Ba–Cu–O thin-films by ionized cluster beam codeposition. *Nuclear Instruments and Methods in Physics Research*, 1989, **B37/38**, 930–934.
9. Swartz, E. T. and Pohl, R. O., Thermal resistances at interfaces. *Applied Physics Letters*, 1987, **51**(26), 2200–2202.
10. Swartz, E. T., Solid-solid thermal boundary resistance. Ph.D. thesis, Cornell University, Ithaca, New York, 1987.
11. Swartz, E. T. and Pohl, R. O., Thermal boundary resistance. *Reviews of Modern Physics*, 1989, **61**(3), 605–668.
12. Little, W. A., The transport of heat between dissimilar solids at low temperatures. *Canadian Journal of Physics*, 1959, **37**, 334–349.
13. Song, Y. and Gaines, J. R., The conductivity threshold for superconductivity in copper oxides: effect of localization and strong correlations. *Journal of Physics: Condensed Matter*, 1991, **3**, 7161–7166.
14. Kashani, A. and Sciver, S. W. V., High heat flux Kapitza conductance of technical copper with several different surface preparations. *Cryogenics*, 1985, **25**, 238–242.
15. Satter, M. and Ashworth, T., An investigation of thermal contact resistance in thermal conductivity measurements of a thin nylon sample. *Thermal Conductivity* 18, ed. Ashworth and Smith. Plenum, New York, 1984, pp. 641–650.
16. Balcevic, J. and Bolsaitis, R., Thermal contact resistance at high heat fluxes. *Heat Transfer—Soviet Research*, 1991, **23**(8), 1017–1033.
17. Fletcher, L. S. Recent developments in contact conductance heat transfer. *Journal of Heat Transfer*, 1988, **110**(4), 1059–1070.
18. Madhusudana, C. V. and Fletcher, L. S., Contact heat transfer—the last decade. *AIAA Journal*, 1986, **24**(3), 510–523.
19. Lambert, M. A. and Fletcher, L. S., Review of the thermal contact conductance of junctions with metallic coatings and films. *Journal of Thermophysics and Heat Transfer*, 1993, **7**(4), 547–554.
20. Mikic, B. B., Thermal contact conductance: theoretical considerations. *International Journal of Heat and Mass Transfer*, 1974, **17**, 205–214.
21. Ochterbeck, J. M., Peterson, G. P. and Fletcher, L. S., Thermal contact conductance of metallic coated BiCaSrCuO superconductor/copper interfaces at cryogenic temperatures. *Journal of Heat Transfer*, 1992, **114**, 21–29.
22. Phelan, P. E. and Ghasemi Nejhad, M. N., Residual stresses for *in situ* deposition of thin-film high-temperature superconductors. *Journal of Electronic Packaging*, 1994, **116**, 249–257.
23. Suhir, E., An approximate analysis of stresses in multilayered elastic thin films. *Journal of Applied Mechanics*, 1988, **55**, 143–148.
24. Tien, C. L., Qiu, T. Q. and Norris, P. M., Microscale thermal phenomena in contemporary technology. *Thermal Science and Engineering, Transactions of the Heat Transfer Society of Japan*, 1994, **2**, 1–11.
25. Richardson, R. A., Peacor, S. D., Uher, C. and Nori, F., $YBa_2Cu_3O_{7-d}$ films: calculation of the thermal conductivity and phonon mean free path. *Journal of Applied Physics*, 1992, **72**(10), 4788–4791.
26. Kittel, C., *Introduction to Solid State Physics*, 6th edn. John Wiley, New York, 1986, pp. 106–108, pp. 515–517.
27. Cheeke, J. D. N., Ettinger, H. and Hebral, B., Analysis of heat transfer between solids at low temperatures. *Canadian Journal of Physics*, 1976, **54**, 1749–1771.